

# The Optical Gravitational Lensing Experiment.

## *UBVI* Photometry of Stars in Baade's Window\*

B. Paczyński<sup>1</sup>, A. Udalski<sup>2</sup>,  
M. Szymański<sup>2</sup>, M. Kubiak<sup>2</sup>,  
G. Pietrzyński<sup>2</sup>, I. Soszyński<sup>2</sup>,  
P. Woźniak<sup>1</sup>, and K. Żebruń<sup>2</sup>

<sup>1</sup> Princeton University Observatory, Princeton, NJ 08544-1001, USA  
e-mail: (bp,wozniak)@astro.princeton.edu

<sup>2</sup>Warsaw University Observatory, Al. Ujazdowskie 4, 00-478 Warszawa,  
Poland

e-mail: (udalski,msz,mk,pietrzyn,soszynsk,zebrun)@sirius.astrouw.edu.pl

### ABSTRACT

We present *UBVI* photometry for 8530 stars in Baade's Window obtained during the OGLE-II microlensing survey. Among these are over one thousand red clump giants. 1391 of them have photometry with errors smaller than 0.04, 0.06, 0.12, and 0.20 mag in the *I*, *V*, *B*, and *U*-band, respectively. We constructed a map of interstellar reddening. The corrected colors of the red clump giants:  $(U - B)_0$ ,  $(B - V)_0$ , and  $(V - I)_0$  are very well correlated, indicating that a single parameter determines the observed spread of their values, reaching almost 2 mag in the  $(U - B)_0$ . It seems most likely that heavy element content is the dominant parameter, but it is possible that another parameter: the age (or mass) of a star moves it along the same trajectory in the color-color diagram as the metallicity. The current ambiguity can be resolved with spectral analysis, and our catalog may be useful as a finding list of red clump giants. We point out that these K giants are more suitable for a fair determination of the distribution of metallicity than brighter M giants.

We also present a compilation of *UBVI* data for 308 red clump giants near the Sun, for which Hipparcos parallaxes are more accurate than 10%. Spectral analysis of their metallicity may provide information about the local metallicity distribution as well as the extent to which mass (age) of these stars affects their colors.

It is remarkable that in spite of a number of problems, stellar models agree with observations at the 0.1–0.2 mag level, making red clump giants not only the best calibrated but also the best understood standard candle.

---

\*Based on observations obtained with the 1.3 m Warsaw telescope at the Las Campanas Observatory of the Carnegie Institution of Washington.

## 1 Introduction

Red clump giants appear to be among the best standard candles available. Not a single RR Lyr star or a Cepheid has its parallax measured by Hipparcos (Perryman *et al.* 1997) with a 10% accuracy (Horner *et al.* 1999), but there are about  $10^3$  red clump giants with parallaxes at least as good as 10% (Paczynski and Stanek 1998). The absolute  $I$ -band magnitude of these stars appears to be almost independent of their  $(V - I)$  color (Paczynski and Stanek 1998). The weak dependence on metallicity was empirically calibrated by Udalski (1998a), who also demonstrated that there is no detectable dependence on age, as long as it is between  $2 \times 10^9$  and  $10 \times 10^9$  years (Udalski 1998b). While this calibration is not perfect, it is superior to the calibration of either RR Lyr or Cepheid variables, or any other standard candle ever proposed. Unfortunately, there is some confusion about the color–metallicity dependence (Paczynski 1998).

The main purpose of this paper is to present a catalog of  $UBVI$  photometry for 8530 stars in Baade’s Window obtained during the second phase of the Optical Gravitational Lensing Experiment (OGLE-II) microlensing project (*cf.* Udalski, Kubiak and Szymański 1997). The important part of the catalog is the list of 1391 red clump giants in the galactic bulge/bar, covering a very broad range of colors, and presumably metallicities. We also present a compilation of  $UBVI$  photometry (Mermilliod and Mermilliod 1994) for 308 nearby red clump giants, for which Hipparcos parallaxes are more accurate than 10%. Our expectation is that these two data sets provide a convenient list of objects for which metallicity can be obtained spectroscopically in order to determine the range of  $[\text{Fe}/\text{H}]$  and  $[\text{O}/\text{H}]$  for nearby stars as well as for those near the Galactic center. Such spectroscopic study could resolve the current ambiguity about the distribution of metallicities and the relation between the metallicity and colors of red clump giants.

We also present, following Kiraga, Paczynski and Stanek (1997), a description of the procedure which appears to be fairly accurate in mapping interstellar extinction. The variation, with the line of sight, of average colors of the bulge red clump stars, red sub-giants, and the stars near the main sequence turn off point are very well correlated with each other, as all are affected by the same variations in the interstellar reddening. The map of color variations provides information about angular scale over which the extinction varies.

## 2 Observations

Observations presented in this paper were collected during the second phase of the OGLE microlensing search with the 1.3-m Warsaw telescope at the Las Campanas Observatory, Chile, which is operated by the Carnegie Institution of Washington. The telescope was equipped with the "first generation" camera with a SITe  $2048 \times 2048$  CCD detector. The pixel size was  $24 \mu\text{m}$  giving the  $0.417$  arcsec/pixel scale. Observations were performed in the "medium" speed reading mode of CCD detector with the gain  $7.1 \text{ e}^-/\text{ADU}$  and readout noise of about  $6.3 \text{ e}^-$ . Details of the instrumentation setup can be found in Udalski, Kubiak and Szymański (1997).

The *BVI* photometry comes from observations of the OGLE-II field covering large part of Baade's Window: BUL\_SC45. Observations of this field were obtained in the drift-scan mode of CCD detector and the field covers approximately  $14.2 \times 57$  arcmin in the sky. Coordinates of its center are:  $\text{RA}(\text{J2000}) = 18^{\text{h}}03^{\text{m}}37$ ,  $\text{DEC}(\text{J2000}) = -30^{\circ}05'00''$ . The effective exposure time was 87, 124 and 162 seconds for the *I*, *V* and *B*-band, respectively. BUL\_SC45 field is observed in somewhat different way than the remaining 47 bulge fields – it is not a subject of microlensing search. Observations of this field are collected mainly for maintaining the phasing of variable stars discovered in its part during the first stage of the OGLE project (*cf.* Udalski *et al.* 1995). Therefore only about 30 *I*-band, 15 *V*-band and 10 *B*-band epochs were collected during the period August 5, 1997 through October 21, 1998.

The *U*-band photometry was obtained in the standard, still frame mode of the CCD detector. One field, covering  $14.2 \times 14.2$  arcmin in the sky and centered approximately at the field BWC of OGLE-I:  $\text{RA}(\text{J2000}) = 18^{\text{h}}03^{\text{m}}24^{\text{s}}$ ,  $\text{DEC}(\text{J2000}) = -30^{\circ}02'00''$ ; (*cf.* Udalski *et al.* 1993, and also Stanek 1996) was observed on four nights between September 20 and September 25, 1998. The field overlaps in large part with BUL\_SC45 field. The exposure time was 1800 seconds.

Observations collected in the drift-scan mode were reduced with the standard OGLE data pipeline and transformed to the *BVI* system based on observations of standard stars from Landolt (1992) fields collected during 5–7 photometric nights (*cf.* Udalski *et al.* 1998b). *U*-band photometry collected in the still-frame mode was reduced in similar manner as described in Udalski (1998b) with the difference that the full  $2048 \times 2048$  pixel image was divided into 16  $512 \times 512$  pixel sub-frames and each of them was reduced separately to ensure constant PSF. In this case transformation to

the standard system was based on photometry of standard stars collected during three photometric nights.

The systematic error of the *BVI*-band transformation should be smaller than 0.02–0.03 mag. For *U*-band the systematic error might be larger and we conservatively assume it to be equal to 0.05 mag. This is caused by somewhat different spectral response of the OGLE instrumental ultraviolet filter because of somewhat steeper cut of the short wavelength ( $\lambda < 3500 \text{ \AA}$ ) side of the *U*-band by the telescope field corrector made from BK7 Schott glass. Nevertheless, the standard stars transform well to the standard system and the color term coefficient for the *U*-band is equal to 0.127 (0.000 means the standard system) which compares to  $-0.041$ ,  $+0.004$  and  $+0.032$  for *B*, *V* and *I*-band, respectively.

The final list of Baade’s Window stars with *UBVI* photometry was constructed by cross-identification of all stars found in the *U*-band images with the stars from the drift-scan field BUL\_SC45 using second order transformation between pixel coordinates.

Astrometric positions of stars were determined with the standard OGLE procedure as described in Udalski *et al.* (1998b). About 10270 stars from the BUL\_SC45 field were used to derive transformation between image pixel coordinates and the Digitized Sky Survey (DSS) coordinate system. Internal accuracy of determined equatorial coordinates is about 0.15 arcsec with possible systematic errors of the DSS system up to 0.7 arcsec.

### 3 *UBVI* Photometry of Baade’s Window Stars

Table 1 contains *UBVI* photometric data for 8530 stars in Baade’s Window. We provide there star ID number (in BUL\_SC45 field), equatorial coordinates (J2000) and observed and extinction-free (see below) *UBVI* magnitudes of each star. Table 1 is too large to be conveniently printed, therefore only a few sample lines are shown. Full versions of Tables presented in this paper are available in electronic form from the OGLE Internet data archive: <http://www.astroww.edu.pl/~ftp/ogle> or its mirror <http://www.astro.princeton.edu/~ogle>.

The  $I - (V - I)$ ,  $I - (B - V)$ , and  $I - (U - B)$  color–magnitude diagrams (CMDs) of Baade’s Window stars are shown in Fig. 1 for 50% of the total of 8530 stars for which *UBVI* band photometry was more accurate than 0.1 mag. The red clump is clearly visible in all three diagrams, and its width increases dramatically toward the blue and ultraviolet. For these

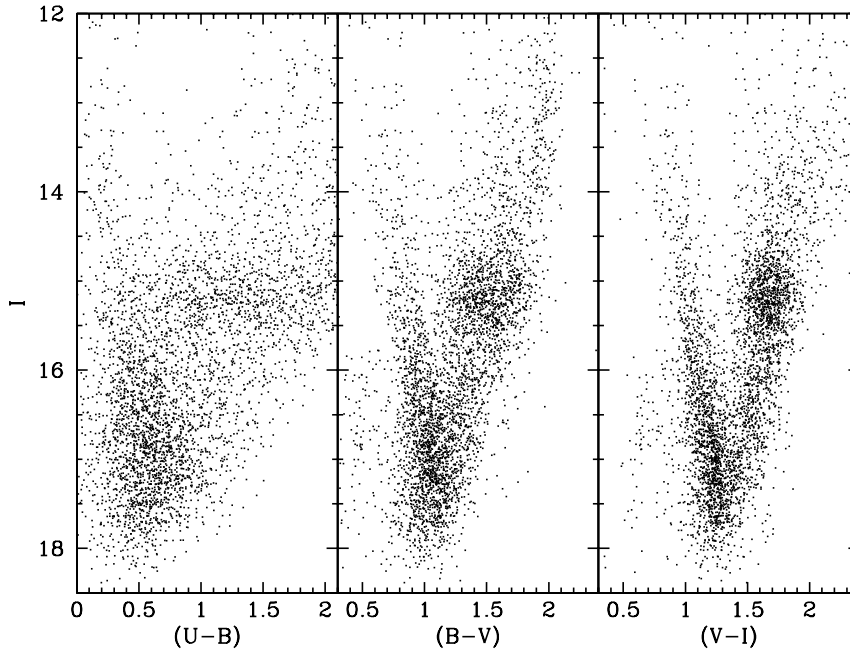


Fig. 1. Color-magnitude diagrams for 50% of the 8530 stars in Baade's Window for which *UBVI* photometry was obtained by the OGLE-II. Photometric errors in all bands are smaller than 0.1 mag. Notice the increase of color range of red clump giants progressing from  $(V - I)$ , through  $(B - V)$  to  $(U - B)$ .

diagrams to be useful we have to correct them for interstellar reddening.

## 4 Reddening Map

We followed Kiraga, Paczyński and Stanek (1997) in the determination of interstellar reddening variation over our field. We selected 38,249 stars for which *V* and *I*-band photometry was more accurate than 0.1 mag. The corresponding CMD for 25% of those stars is shown in Fig. 2. Four regions were selected: one near the red clump (RC), one below it, at the red giant branch (RG), and two near the main sequence turn off point, one brighter, and the other one fainter (TOPb, TOPf), as indicated in Fig. 2. The six parallel lines are described with the equations:  $I - 1.5 \times (V - I) = C$ , where  $C = 12.00, 13.25, 14.50, 15.50, 16.00, 16.50$ , respectively. The slope of these lines was chosen so that they are parallel to the reddening vector (Stanek 1996).

Table 1  
*UBVI* photometry of 8530 stars in Baade's Window

Star no BUL_SC45	RA (J2000)	DEC (J2000)	$U$	$\sigma_U$	$B$	$\sigma_B$	$V$	$\sigma_V$	$I$	$\sigma_I$	$U_0$	$B_0$	$V_0$	$I_0$
58901	18 <sup>h</sup> 03 <sup>m</sup> 13 <sup>s</sup> 32	-30° 08' 54.''5	17.590	0.025	15.468	0.026	13.689	0.014	11.792	0.012	14.660	13.001	11.839	10.682
58903	18 <sup>h</sup> 03 <sup>m</sup> 11 <sup>s</sup> 96	-30° 08' 37.''6	19.976	0.055	17.409	0.029	15.296	0.027	12.473	0.015	17.082	14.972	13.468	11.376
58904	18 <sup>h</sup> 03 <sup>m</sup> 12 <sup>s</sup> 59	-30° 08' 34.''1	19.574	0.025	17.125	0.052	15.052	0.061	11.930	0.050	16.741	14.739	13.263	10.856
58930	18 <sup>h</sup> 03 <sup>m</sup> 20 <sup>s</sup> 14	-30° 08' 50.''0	17.925	0.014	16.610	0.021	15.024	0.010	13.100	0.010	15.213	14.326	13.311	12.072
58934	18 <sup>h</sup> 03 <sup>m</sup> 18 <sup>s</sup> 49	-30° 08' 39.''5	16.441	0.022	15.866	0.030	14.818	0.022	13.565	0.027	13.746	13.597	13.116	12.544
58935	18 <sup>h</sup> 03 <sup>m</sup> 14 <sup>s</sup> 29	-30° 08' 34.''3	17.747	0.021	15.952	0.012	14.365	0.014	12.689	0.011	15.016	13.652	12.640	11.654
58936	18 <sup>h</sup> 03 <sup>m</sup> 19 <sup>s</sup> 42	-30° 08' 34.''5	20.479	0.084	18.346	0.024	16.335	0.028	12.954	0.013	17.797	16.087	14.641	11.938
58999	18 <sup>h</sup> 03 <sup>m</sup> 15 <sup>s</sup> 20	-30° 08' 50.''7	19.923	0.037	17.884	0.023	16.044	0.008	13.948	0.010	17.248	15.632	14.355	12.934
59000	18 <sup>h</sup> 03 <sup>m</sup> 11 <sup>s</sup> 04	-30° 08' 50.''2	19.223	0.039	17.536	0.028	15.914	0.011	14.137	0.011	16.222	15.009	14.019	13.000
59001	18 <sup>h</sup> 03 <sup>m</sup> 18 <sup>s</sup> 83	-30° 08' 48.''8	15.904	0.010	15.728	0.015	15.066	0.009	14.193	0.009	13.199	13.450	13.358	13.168
59002	18 <sup>h</sup> 03 <sup>m</sup> 12 <sup>s</sup> 46	-30° 08' 42.''3	16.464	0.003	16.029	0.013	15.103	0.017	13.912	0.011	13.544	13.570	13.259	12.805
59003	18 <sup>h</sup> 03 <sup>m</sup> 19 <sup>s</sup> 52	-30° 08' 42.''0	15.481	0.001	15.276	0.016	14.844	0.013	14.236	0.008	12.775	12.997	13.135	13.211
59174	18 <sup>h</sup> 03 <sup>m</sup> 14 <sup>s</sup> 44	-30° 08' 45.''3	20.348	0.089	19.494	0.087	17.178	0.059	15.253	0.016	17.575	17.158	15.426	14.202
59175	18 <sup>h</sup> 03 <sup>m</sup> 09 <sup>s</sup> 10	-30° 08' 44.''1	21.456	0.023	19.085	0.050	17.187	0.021	15.132	0.012	18.402	16.514	15.258	13.975
59176	18 <sup>h</sup> 03 <sup>m</sup> 04 <sup>s</sup> 49	-30° 08' 40.''6	19.844	0.060	18.611	0.030	17.137	0.071	15.243	0.021	16.922	16.150	15.291	14.136
59177	18 <sup>h</sup> 03 <sup>m</sup> 14 <sup>s</sup> 35	-30° 08' 41.''0	21.223	0.098	18.762	0.033	16.946	0.011	15.041	0.011	18.459	16.434	15.200	13.993
59178	18 <sup>h</sup> 03 <sup>m</sup> 13 <sup>s</sup> 91	-30° 08' 39.''6	17.426	0.013	16.765	0.021	15.818	0.013	14.713	0.015	14.622	14.404	14.047	13.650
59180	18 <sup>h</sup> 03 <sup>m</sup> 10 <sup>s</sup> 00	-30° 08' 33.''7	16.719	0.007	16.356	0.014	15.660	0.021	14.631	0.020	13.707	13.819	13.757	13.489
59494	18 <sup>h</sup> 03 <sup>m</sup> 07 <sup>s</sup> 90	-30° 08' 51.''8	20.342	0.007	19.215	0.055	17.806	0.018	16.121	0.020	17.298	16.651	15.883	14.967

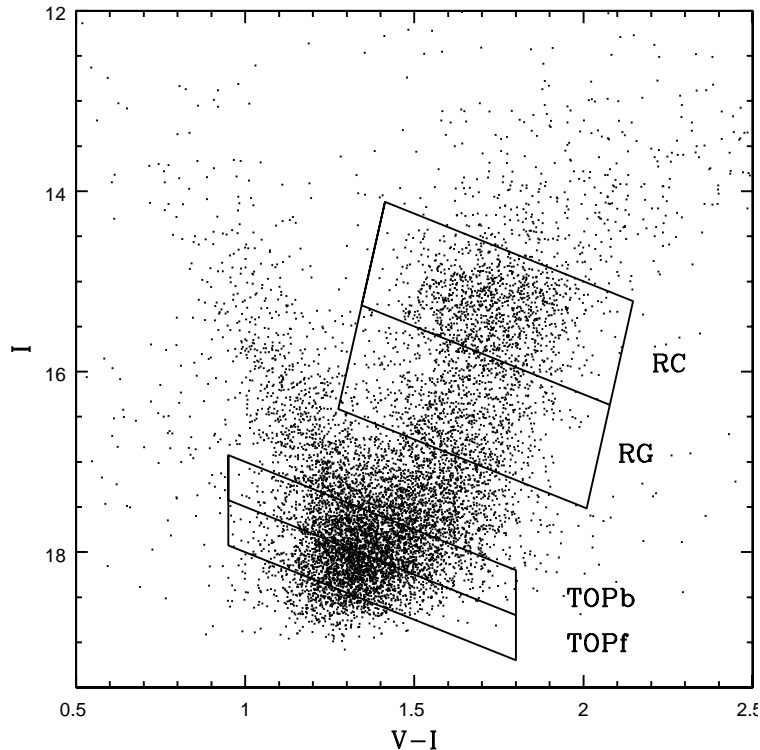


Fig. 2. Color-magnitude diagram for 25% of the 38,249 stars in Baade’s Window for which  $V$  and  $I$ -band photometry was obtained by the OGLE-II. Photometric errors in both bands are smaller than 0.1 mag. The stars in the four marked regions were used for reddening determination.

We divided our field into squares of  $200 \times 200$  pixels. In every square we calculated average color of the stars in each of the four groups separately, and also the average of the stars in all four groups. It is safe to assume that there was no significant variation in stellar populations within our field, which had the total area of only  $(0.23)^2$ . The variation of average colors was due to variation in the interstellar reddening as well as the statistical fluctuations caused by a small number of stars.

The colors of all four stellar groups are very well correlated, as shown in Fig. 3. To bring the colors of the four groups to the same average value the corrections were added to the  $(V-I)$  color of each star, with  $\Delta(V-I)_{\text{TOPf}} = +0.200$  mag,  $\Delta(V-I)_{\text{TOPb}} = +0.138$  mag,  $\Delta(V-I)_{\text{RG}} = -0.120$  mag and  $\Delta(V-I)_{\text{RC}} = -0.217$  mag. The shift between colors of each group in Fig. 3 has been increased for the clarity of presentation.

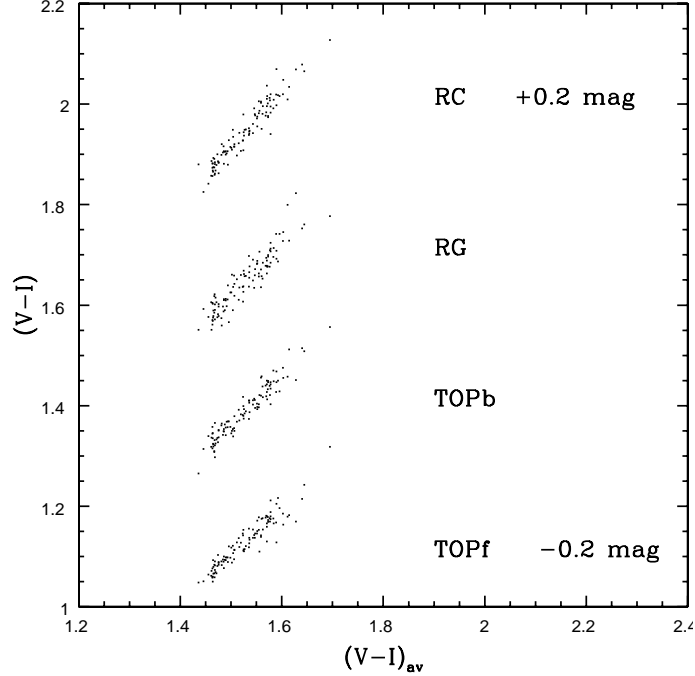


Fig. 3. Relation between the average  $(V-I)$  colors of the stars in four areas indicated in Fig. 2 are shown as a function of the average  $(V-I)_{av}$  for stars in all four areas. Each dot corresponds to a different square in the CCD field,  $200 \times 200$  pixels, *i.e.*,  $83''.4 \times 83''.4$  each.

As there was such a good correlation between the colors of the four groups we combined all stars, adding the suitable corrections as given above. We calculated average colors for the stars in squares  $50 \times 50$  pixels, *i.e.*,  $20''.8 \times 20''.8$  in the sky. The total number of such squares in our field was  $39 \times 42 = 1638$ . These became our resolution elements for the reddening map, or the elementary squares. The number of stars in the four groups was:  $N_{TOPf} = 6422$ ,  $N_{TOPb} = 7776$ ,  $N_{RG} = 4185$ ,  $N_{RC} = 4546$ . The total number of all stars used for the reddening determination was  $N = 22,929$ , the average number of stars per elementary square was  $n = 14.0$ , and the variance of the average color was  $\langle \sigma_{V-I}^2 \rangle = (0.034 \text{ mag})^2$ . The *rms* variation of the  $(V-I)$  color per star was approximately 0.13 mag.

Given the values of the average  $(V-I)$  colors in 1638 elementary squares we calculated the correlation function defined as

$$\sigma^2(d) = \langle \Delta(V-I)^2 \rangle, \quad (1)$$



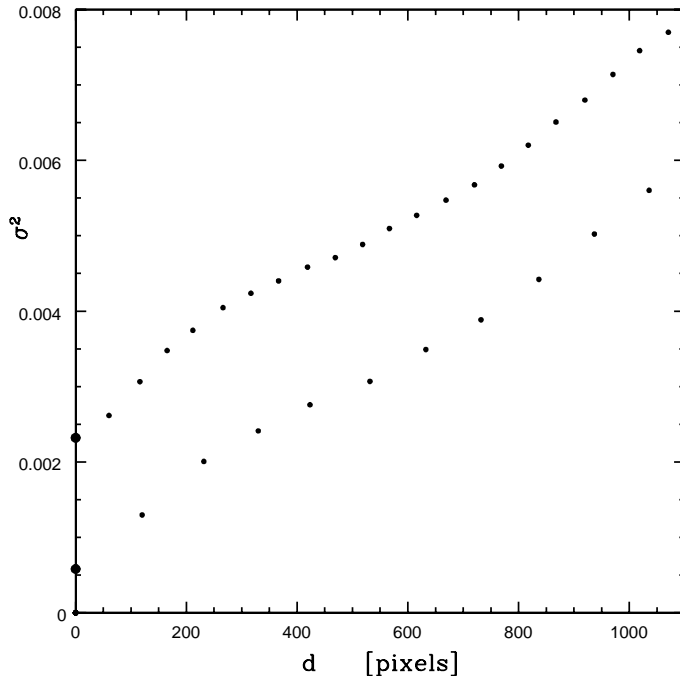


Fig. 4. Correlation function  $\sigma^2$  of the variation in  $(V-I)$  is shown as a function of separation  $d$ . The upper sequence of points corresponds to the resolution  $50 \times 50$  pixels, while the lower sequence corresponds to the resolution  $100 \times 100$  pixels.

averaged over all pairs of squares within each range of separations  $d$ .  $\sigma^2$  is shown in Fig. 4 as a function of the separation between the elementary squares (the upper sequence of points). The point corresponding to the separation  $d=0$  is twice the variance of the  $(V-I)$  color per elementary square. Fig. 4 shows that the value of the correlation function doubles at a separation  $d \approx 500$  pixels, which is 10 times larger than the elementary square size. We repeated the exercise by combining 4 adjacent elementary squares into one composite square of  $100 \times 100$  pixels, thereby increasing the average number of stars to 56.0, and reducing the variance of the average  $(V-I)$  color to  $(0.017 \text{ mag})^2$ . The corresponding correlation points are shown as the lower sequence in Fig. 4. This time the correlation function doubles its value at a separation  $d \approx 100$  pixels.

While the zero point depends on the choice of the square size, the rest of the correlation function is the same in both cases, except for the zero point shift. The contribution of interstellar reddening to the correlation function

may be approximated as

$$\langle \Delta E_{V-I}^2 \rangle \approx (0.027 \text{ mag})^2 \times \frac{d}{1'}, \quad 0 < d < 7'. \quad (2)$$

How to choose the right square size? If the squares are small then the resolution is high, and the variations of interstellar reddening from square to square are small. However, there are few stars per square and the statistical error in the estimate of the average stellar color is large. When the squares are large the opposite is true: the average color is calculated accurately, but the resolution is poor and the variations of the interstellar reddening within the square become substantial. Without attempting a rigorous analysis it seems that a sensible square size is such, that the two contributions: the random noise due to a finite number of stars within the square, and the variations of the interstellar reddening within the square are comparable. Fig. 4 suggests that a sensible choice is a square size  $100 \times 100$  pixels, *i.e.*,  $41''.7 \times 41''.7$  in the sky.

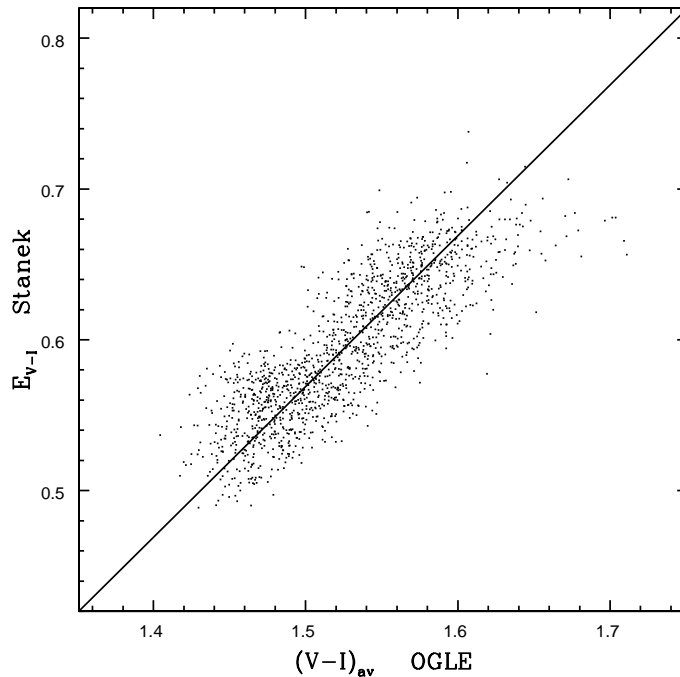


Fig. 5. Correlation of the average color  $(V-I)_{\text{av}}$  of the OGLE stars on the reddening  $E_{V-I}$  calculated with Stanek's (1996) map. The diagonal line is the relation:  $(V-I)_{\text{av}} = E_{V-I} + 0.931$ .

We calculated average  $(V - I)_{\text{av}}$  color for the stars in a grid of  $100 \times 100$  pixel squares. We shifted the grid by 50 pixels in both directions, so as to have average color calculated at 50 pixel intervals. A comparison between the  $(V - I)_{\text{av}}$  color from our data and the color excess  $E_{V-I}$  calculated with the Stanek's (1996) extinction map is shown in Fig. 5. The agreement is good, and we adopt the relation:

$$E_{V-I} = (V - I)_{\text{av}} - 0.931, \quad \langle E_{V-I} \rangle = 0.59. \quad (3)$$

Obviously, our method, as well as Stanek's, provides only a differential reddening map. The zero point adopted by Stanek, and therefore also by us, is based on the determination by Gould *et al.* (1998) and Alcock *et al.* (1998).

We calculate reddening within our  $(0^\circ 23')^2$  field by linear interpolation in the grid with the spacing of 50 pixels. The values of  $E_{V-I}$  are based on the average  $(V - I)_{\text{av}}$  calculated in  $100 \times 100$  pixel squares. Therefore, the resolution of our extinction map is 100 pixels, *i.e.*,  $41''7$  in the sky. We estimate the statistical accuracy of our reddening map to be  $\approx 0.02$  mag. Of course, the uncertainty in the zero point of our extinction is substantially larger. The FORTRAN code RED.F, calculating reddening within our field is available from the OGLE Internet archive.

## 5 Color–Color Diagrams

The extinction in the four bands was calculated according to the formulae:

$$A_I = 1.500 \cdot E_{V-I}, \quad \langle A_I \rangle = 0.88, \quad (4a)$$

$$A_V = 2.500 \cdot E_{V-I}, \quad \langle A_V \rangle = 1.48, \quad (4b)$$

$$A_B = 3.333 \cdot E_{V-I}, \quad \langle A_B \rangle = 1.97, \quad (4c)$$

$$A_U = 3.958 \cdot E_{V-I}, \quad \langle A_U \rangle = 2.34, \quad (4d)$$

and the colors were corrected for the reddening accordingly. The coefficients in the Eqs. (4a)–(4d) are more or less standard, but the reader may adopt different values as we provide the original as well as the dereddened photometry. The reddening varied relatively little over our small field of view, with 90% of stars in the range  $0.51 < E_{V-I} < 0.65$ . Therefore, the CMDs corrected for extinction were similar to those shown in Fig. 1, except for a shift in color and magnitude.

Table 2  
*UBVI* photometry of 1391 red clump giants in Baade's Window

Star no BUL_SC45	RA (J2000)	DEC (J2000)	$U$	$\sigma_U$	$B$	$\sigma_B$	$V$	$\sigma_V$	$I$	$\sigma_I$	$U_0$	$B_0$	$V_0$	$I_0$
59174	18 <sup>h</sup> 03 <sup>m</sup> 14 <sup>s</sup> .44	-30° 08' 45."3	20.348	0.089	19.494	0.087	17.178	0.059	15.253	0.016	17.575	17.159	15.426	14.202
67536	18 <sup>h</sup> 03 <sup>m</sup> 19 <sup>s</sup> .06	-30° 08' 11."2	19.098	0.022	18.279	0.060	16.913	0.031	15.317	0.035	16.494	16.086	15.268	14.330
67556	18 <sup>h</sup> 03 <sup>m</sup> 04 <sup>s</sup> .12	-30° 07' 51."4	18.596	0.038	18.287	0.111	16.740	0.010	15.197	0.033	16.067	16.157	15.143	14.239
67577	18 <sup>h</sup> 03 <sup>m</sup> 19 <sup>s</sup> .24	-30° 07' 36."1	20.056	0.104	18.630	0.037	17.005	0.016	15.184	0.021	17.378	16.375	15.313	14.169
67584	18 <sup>h</sup> 03 <sup>m</sup> 06 <sup>s</sup> .19	-30° 07' 27."2	19.693	0.053	18.325	0.054	16.754	0.012	15.017	0.012	17.234	16.254	15.201	14.085
67591	18 <sup>h</sup> 03 <sup>m</sup> 10 <sup>s</sup> .00	-30° 07' 21."1	20.127	0.066	18.760	0.096	16.888	0.008	15.071	0.017	17.565	16.602	15.270	14.100
67593	18 <sup>h</sup> 03 <sup>m</sup> 16 <sup>s</sup> .02	-30° 07' 15."9	20.629	0.050	18.570	0.050	16.812	0.011	15.031	0.008	18.156	16.488	15.250	14.094
67596	18 <sup>h</sup> 03 <sup>m</sup> 08 <sup>s</sup> .62	-30° 07' 13."6	21.077	0.151	18.905	0.086	17.211	0.036	15.438	0.040	18.484	16.722	15.573	14.455
67598	18 <sup>h</sup> 03 <sup>m</sup> 12 <sup>s</sup> .28	-30° 07' 12."7	18.681	0.020	17.930	0.024	16.623	0.016	15.076	0.009	16.256	15.888	15.092	14.157
67604	18 <sup>h</sup> 03 <sup>m</sup> 19 <sup>s</sup> .98	-30° 07' 09."3	20.717	0.061	19.043	0.031	17.313	0.023	15.347	0.011	18.096	16.836	15.657	14.354
67607	18 <sup>h</sup> 03 <sup>m</sup> 08 <sup>s</sup> .14	-30° 07' 07."7	20.008	0.035	18.584	0.068	17.007	0.031	15.256	0.014	17.423	16.407	15.374	14.276
67609	18 <sup>h</sup> 03 <sup>m</sup> 15 <sup>s</sup> .89	-30° 07' 06."4	20.042	0.111	18.623	0.033	17.124	0.016	15.423	0.012	17.596	16.563	15.579	14.496
67610	18 <sup>h</sup> 03 <sup>m</sup> 16 <sup>s</sup> .75	-30° 07' 06."5	19.684	0.079	18.697	0.059	16.977	0.018	15.366	0.019	17.187	16.594	15.400	14.420
67614	18 <sup>h</sup> 03 <sup>m</sup> 06 <sup>s</sup> .27	-30° 07' 02."0	20.911	0.126	18.890	0.069	17.140	0.012	15.348	0.020	18.425	16.796	15.570	14.406
67616	18 <sup>h</sup> 03 <sup>m</sup> 16 <sup>s</sup> .78	-30° 06' 57."9	20.316	0.012	18.604	0.040	16.996	0.013	15.226	0.015	17.829	16.510	15.425	14.284
67617	18 <sup>h</sup> 03 <sup>m</sup> 13 <sup>s</sup> .92	-30° 06' 56."5	18.784	0.014	18.152	0.047	16.550	0.017	15.020	0.018	16.373	16.122	15.027	14.106
67618	18 <sup>h</sup> 03 <sup>m</sup> 19 <sup>s</sup> .06	-30° 06' 57."0	20.810	0.167	18.864	0.044	17.165	0.021	15.285	0.012	18.217	16.681	15.527	14.302
67619	18 <sup>h</sup> 03 <sup>m</sup> 05 <sup>s</sup> .45	-30° 06' 56."1	20.552	0.195	18.970	0.085	17.058	0.018	15.223	0.019	18.114	16.917	15.518	14.299
67620	18 <sup>h</sup> 03 <sup>m</sup> 09 <sup>s</sup> .55	-30° 06' 52."0	20.913	0.165	18.852	0.114	16.963	0.011	15.104	0.015	18.417	16.750	15.387	14.158

Table 3  
Hipparcos red clump giants

Hipparcos no	RA (J2000)	DEC (J2000)	$(V - I)$	$(B - V)$	$(U - B)$	$V$	$M_V$	$M_I$	$d$ [pc]
671	0 <sup>h</sup> 08 <sup>m</sup> 17 <sup>s</sup> .55	-8° 49' 26.''5	0.990	1.035	0.828	5.985	0.944	-0.046	102.14
765	0 <sup>h</sup> 09 <sup>m</sup> 24 <sup>s</sup> .54	-45° 44' 49.''2	1.000	1.024	0.843	3.872	0.715	-0.285	42.96
814	0 <sup>h</sup> 10 <sup>m</sup> 02 <sup>s</sup> .27	-82° 13' 26.''4	0.980	1.050	0.925	5.268	0.934	-0.046	74.35
966	0 <sup>h</sup> 11 <sup>m</sup> 56 <sup>s</sup> .13	-42° 10' 19.''3	1.010	1.040	0.840	6.530	1.037	0.027	125.47
2568	0 <sup>h</sup> 32 <sup>m</sup> 35 <sup>s</sup> .40	20° 17' 40.''0	1.000	1.069	0.956	5.367	0.897	-0.103	78.80
2926	0 <sup>h</sup> 37 <sup>m</sup> 07 <sup>s</sup> .20	24° 00' 51.''3	1.080	1.179	1.269	6.171	1.125	0.045	102.56
3031	0 <sup>h</sup> 38 <sup>m</sup> 33 <sup>s</sup> .50	29° 18' 44.''5	0.920	0.871	0.466	4.360	0.772	-0.148	51.71
3092	0 <sup>h</sup> 39 <sup>m</sup> 19 <sup>s</sup> .60	30° 51' 40.''4	1.230	1.279	1.484	3.263	0.809	-0.421	31.07
3137	0 <sup>h</sup> 39 <sup>m</sup> 51 <sup>s</sup> .91	-44° 47' 46.''8	1.060	1.144	1.090	6.005	1.157	0.097	93.02
3455	0 <sup>h</sup> 44 <sup>m</sup> 11 <sup>s</sup> .41	-10° 36' 33.''4	0.980	1.015	0.843	4.756	0.727	-0.253	64.35
3456	0 <sup>h</sup> 44 <sup>m</sup> 11 <sup>s</sup> .92	-38° 25' 19.''1	1.070	1.142	1.181	5.877	0.613	-0.457	114.15
3781	0 <sup>h</sup> 48 <sup>m</sup> 35 <sup>s</sup> .12	-74° 55' 24.''1	1.340	1.368	1.674	5.061	1.102	-0.238	62.74
4257	0 <sup>h</sup> 54 <sup>m</sup> 17 <sup>s</sup> .58	-8° 44' 26.''0	0.910	0.916	0.533	6.163	0.822	-0.088	116.28
4422	0 <sup>h</sup> 56 <sup>m</sup> 40 <sup>s</sup> .01	59° 10' 52.''2	1.010	0.955	0.679	4.627	0.619	-0.391	63.13
4587	0 <sup>h</sup> 58 <sup>m</sup> 43 <sup>s</sup> .89	-11° 22' 47.''8	0.960	0.942	0.672	5.618	0.695	-0.265	96.62
5170	1 <sup>h</sup> 06 <sup>m</sup> 07 <sup>s</sup> .73	-23° 59' 32.''5	1.020	1.079	1.002	6.137	0.965	-0.055	107.41
5364	1 <sup>h</sup> 08 <sup>m</sup> 35 <sup>s</sup> .26	-10° 10' 54.''9	1.110	1.161	1.190	3.441	0.675	-0.435	36.06
5485	1 <sup>h</sup> 10 <sup>m</sup> 11 <sup>s</sup> .96	-8° 54' 21.''7	0.980	1.032	0.880	6.391	1.157	0.177	111.86
5586	1 <sup>h</sup> 11 <sup>m</sup> 39 <sup>s</sup> .59	30° 05' 23.''0	1.050	1.092	1.011	4.509	1.027	-0.023	49.73

Median errors of the OGLE-II photometry of the red clump giants are 0.016, 0.02, 0.04 and 0.06 mag for  $I$ ,  $V$ ,  $B$  and  $U$ -band, respectively. The  $I$ -band errors are color independent, but the errors in  $V$ ,  $B$  and mostly in  $U$ -band increase with the  $(V - I)$  color, because the redder stars are fainter. In the  $U$ -band the reddest red clump stars are near our detection limit, as it is apparent in Fig. 1. We rejected stars with the errors larger than 0.04, 0.06, 0.12, and 0.20 mag in the  $I$ ,  $V$ ,  $B$  and  $U$ -band, respectively; these were about 5% of the total. 1391 stars had smaller photometric errors and satisfied the inequalities:

$$14.0 < I_0 < 14.5, \quad 0.8 < (V - I)_0 < 1.6, \quad (5)$$

and these are listed in Table 2 (full version is available from the OGLE Internet archive). Note, that some stars in Table 2 are not present in Table 1, because the criteria used for the error discrimination were different for the two sets.

We also selected red clump giants from the Hipparcos catalog according to the following criteria: genuine  $I$ -band photometry was available in the catalog, the absolute magnitude  $M_I$ , the color  $(V - I)$ , and the parallax  $\pi$  satisfied the criteria:

$$-0.5 < M_I < 0.2, \quad 0.8 < (V - I) < 1.6, \quad \pi \text{ error} < 10\%, \quad (6)$$

J-C. Mermilliod kindly provided us with the  $UBV$  photometry for the selected stars in a computer readable form (*cf.* Mermilliod and Mermilliod 1994, and <http://obswww.unige.ch/gcpd/>). The list of 308 stars which satisfied the criteria given above, had  $UBVI$  photometry and had the differences in  $V$  and  $B$  magnitudes as given by the Hipparcos/Tycho catalogs and by Mermilliod not larger than 0.03 mag, are listed in Table 3 (full version is available from the OGLE Internet archive). As all Hipparcos stars with accurate parallaxes are within about 100 pc, their reddening is very small (Stanek and Garnavich 1998, Sekiguchi and Fukugita 1999).

The number of red clump giants for which Hipparcos provides accurate parallaxes is several times larger than 308, and they all have accurate  $V$  and  $B$  photometry, but a large fraction does not have either  $I$  or  $U$  data. The calibration of red clump giants could be improved considerably if standard  $I$  and  $U$  photometry were made for these bright stars.

Figs. 6 and 7 show  $(V - I)_0 - (B - V)_0$  and  $(B - V)_0 - (U - B)_0$  color-color diagrams constructed for 1391 Baade's Window red clump giants. Figs. 8 and 9 show similar diagrams for the Hipparcos sample of red clump

stars. The arrow pointing the direction of interstellar reddening is shown in Figs. 6 and 7, with the filled circles indicating the average reddening, and the open circles indicating the full range of reddening within our field.

## 6 Discussion

### 6.1 *UBVI* Observations

A comparison of several hundred red clump giants for which OGLE-I photometry (Szymański *et al.* 1996) and the current OGLE-II photometry are available allowed us to determine a small offset between the two. The OGLE-I *V*-band is 0.021 mag fainter, the *I*-band is 0.035 mag brighter, and the  $(V - I)$  color is 0.056 mag redder than the corresponding quantities determined with the OGLE-II, which we consider to be more accurate.

The average colors for the red clump giants presented in Table 2, and the *rms* deviations of the stars from the average are: (1.114, 0.117), (1.081, 0.191), and (1.148, 0.510) for  $(V - I)_0$ ,  $(B - V)_0$ , and  $(U - B)_0$ , respectively. The corresponding numbers for the Hipparcos red clump giants listed in Table 3 are: (1.021, 0.091), (1.050, 0.102), and (0.916, 0.239) for these colors. Notice that the range of colors for Baade’s Window stars is larger than for Hipparcos stars, and the difference increases strongly toward short wavelengths, being the largest in  $(U - B)_0$ , as expected for a population with a larger range of metallicities.

We may compare our mean  $(V - I)_0$  colors and their range with the corresponding numbers given by Paczyński and Stanek (1998): (1.16, 0.14) for Baade’s Window (based on OGLE-I data but corrected to the OGLE-II photometric system) and (1.01, 0.08) for the Hipparcos stars. Our new Hipparcos numbers are practically the same as those of Paczyński and Stanek (1998), but there is some difference for Baade’s Window stars. There may be several reasons: Paczyński and Stanek (1998) used a much larger area in their study, with a larger range of interstellar extinction. OGLE-I photometric errors were larger which may be responsible for the apparent larger range of colors, in addition to the systematic offset between OGLE-I and OGLE-II, which has been allowed for.

The data we present in this paper cannot by itself resolve the current ambiguity about the relation between the colors and the metallicity of red clump giants (Paczyński 1998). However, the catalogs of these stars in Baade’s Window (Table 2) and near the Sun (Table 3) can be used to select stars over the full range of colors for spectroscopic studies.

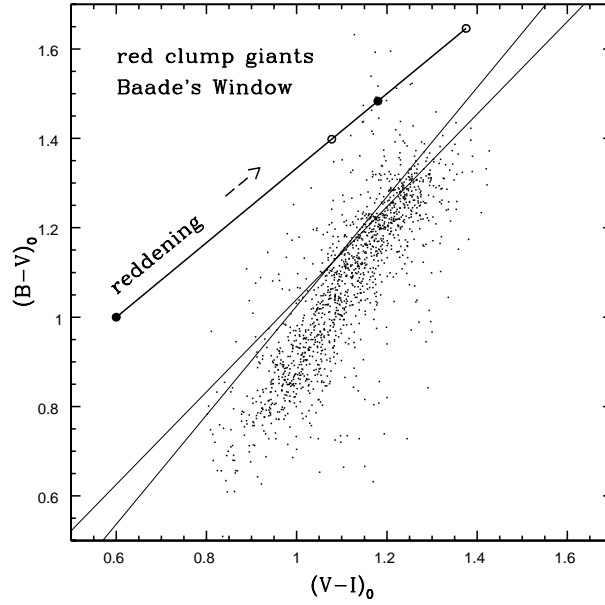


Fig. 6. Color-color diagram:  $(V-I)_0 - (B-V)_0$  for 1391 red clump giants in Baade's Window corrected for interstellar reddening. The two thin lines that cross are for reference; they are the same as in Fig. 8.

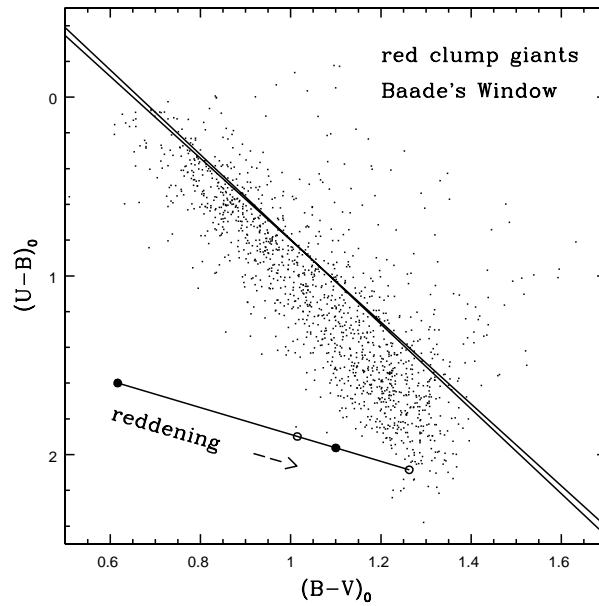


Fig. 7. Color-color diagram:  $(B-V)_0 - (U-B)_0$  for 1391 red clump giants in Baade's Window corrected for interstellar reddening. The two thin lines that cross are for reference; they are the same as in Fig. 9.



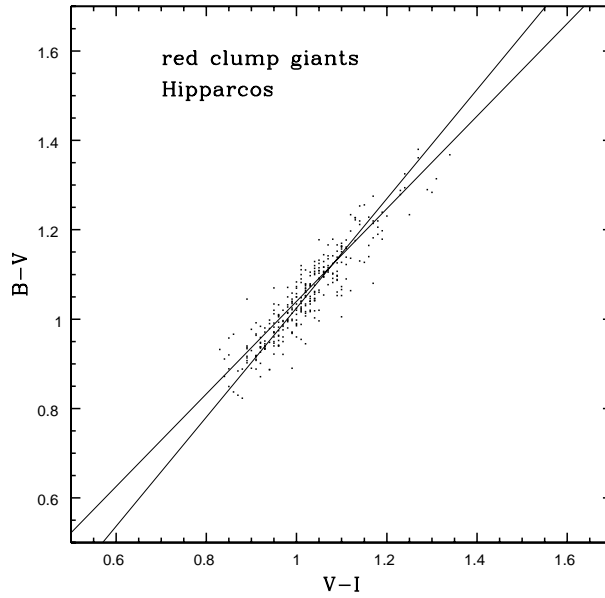


Fig. 8. Color-color diagram:  $(V - I) - (B - V)$  for 308 red clump giants for which Hipparcos measured parallaxes with the accuracy better than 10%. The two thin lines that cross are the regression lines of one color with respect to another.

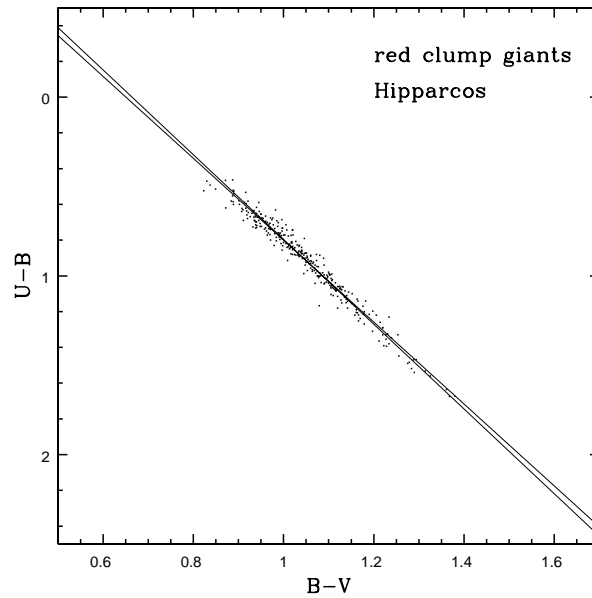


Fig. 9. Color-color diagram:  $(B - V) - (U - B)$  for 308 red clump giants for which Hipparcos measured parallaxes with the accuracy better than 10%. The two thin lines that cross are the regression lines of one color with respect to another.

Tight color–color relations apparent for the Hipparcos stars (Figs. 8 and 9) clearly indicate that either there is a single parameter that determines the red clump colors, or there is a degeneracy between several parameters, which conspire to change stellar colors in the same direction in the three dimensional space of  $(V - I) - (B - V) - (U - B)$ . The same appears to be true for the red clump giants in Baade’s Window (Figs. 6 and 7). The scatter is larger in Baade’s Window for at least two reasons: photometric errors are larger than for the bright Hipparcos stars, and reddening corrections are not perfect. It is somewhat disturbing that the slope of the  $(B - V)_0 - (V - I)_0$  relation is somewhat different for the stars in Baade’s Window than those near the Sun. In principle there is a possibility that the reddening vector varies significantly with the stellar color, but we did not make an estimate of this effect.

If future spectroscopic determinations of the metallicity establish only a weak correlation with colors of red clump giants, then it will be clear that another parameter, most likely the mass (*i.e.*, age) of a star affects its colors too. This would imply that red clump giants make large loops in the CMD during their core helium burning phase. However, if it turns out that the spectroscopic metallicity is very well correlated with colors, then the implication will be that the dependence on mass (age) is weak, and the evolutionary loops are small.

Note, that our samples of the red clump giants are not likely to be biased by their colors, as they are all well above the detection limit, except for the reddest stars, for which  $U$ -band magnitude was close to the detection limit (*cf.* Fig. 1).

Following the approach of Paczyński and Stanek (1998) we determined that the number density of red clump stars peaks at  $I_0 = 14.37 \pm 0.02$ . Of course, the true error may be as large as 0.1 mag because the zero point of the interstellar extinction is uncertain (Alcock *et al.* 1998, Gould *et al.* 1998). For comparison, Paczyński and Stanek (1998) obtained  $I_0 = 14.36$  for the peak of the red clump stars, allowing for the systematic offset between OGLE-I and OGLE-II.

Stanek *et al.* (1999) have presented  $UBVI$  photometry in a nearby field BW8 in Baade’s Window. Their results are in substantial agreement with ours, although there appear to be some systematic differences of order of 0.05 mag in zero points of photometry. They also discuss the effect of metallicity on colors of the red clump stars.

## 6.2 Stellar Models

It is remarkable how well the models of red clump giants agree with the observations. Recently, evolutionary tracks for a broad range of metallicities and masses were calculated by Bertelli *et al.* (1994), Jimenez, Flynn and Kotoneva (1998), and by Girardi *et al.* (1998). The results are best summarized by Fig. 1 of Girardi *et al.* (1998), which clearly shows that the absolute *I*-band magnitude changes very little with stellar mass (*i.e.*, age), but it decreases by 0.2–0.3 mag when the metallicity decreases from  $Z = 0.03$  to  $Z = 0.001$ , in a fairly good agreement with the Udalski’s (1998b) empirical calibration. Models demonstrate that while the metallicity is the dominant factor affecting the colors, the stellar mass (age) makes a non-negligible contribution, especially at high metallicities, where red clump giants make fairly large horizontal loops in the CMD. This suggests that there is some degeneracy, in the sense that metallicity and stellar mass (age) move a star along nearly the same, approximately horizontal vector in the CMD, and along approximately the same vector in a color–color diagram.

Things are different at very low metallicities, like those found in Leo I (Caputo *et al.* 1999), where  $Z = 0.0004$  or even 0.0001. Under these extreme conditions the red clump appears like a small arc, with the top and bottom relatively blue, and the middle relatively red. The range of luminosities of the red clump giants in Leo I is larger than the range observed in the Galaxy (*e.g.*, Paczyński and Stanek 1998), Magellanic Clouds (*e.g.*, Udalski *et al.* 1998a, Stanek, Zaritsky and Harris 1998), or in M31 (Stanek and Garnavich 1998). This is in excellent agreement with the prediction of stellar evolutionary models (Bertelli *et al.* 1994), and indicates a very large spread in masses (ages) of the extremely metal poor population observed in Leo I (Caputo *et al.* 1999).

Things are also different for very young red clump giants, as it is apparent in the data (Udalski *et al.* 1998a) and in the models (*cf.* Fig. 1 of Girardi *et al.* 1998): the stars younger than 2 Gyr are brighter than those in the age group of 2–10 Gyr. However, it is remarkable, that in all objects with a large number of red clump giants that were studied so far: Hipparcos stars and the Galactic bulge (Paczyński and Stanek 1998), LMC, SMC, Carina dwarf galaxy (Udalski *et al.* 1998a, Udalski 1998a), M31 (Stanek and Garnavich 1998), the red clump shows very little spread in the *I*-band magnitude, indicating that the stellar population is dominated by stars which are 2–10 Gyr old.

While one may argue about 0.1 mag or even 0.2 mag discrepancy between

the models and observations (*e.g.*, Girardi 1999), the situation is comparable to, or better than, the situation with the RR Lyr stars or with Cepheids, except those stars do not have empirical calibration as good as the red clump giants. A thorough comparison between the models and the data for the red clump giants can be found in Stanek *et al.* (1999).

While the evolutionary models are in a reasonable agreement with observations, one should be aware of several problems with the models which cannot be readily resolved and which make a perfect agreement with the data almost impossible.

It is well known that theory cannot predict what should be the value of the mixing length parameter which is used to describe non-adiabatic convection below stellar photosphere. Moreover, the model effective temperature and radius are very sensitive to this parameter, and in practice the calibration is empirical. There is no reason for the mixing length parameter to be a universal constant, and today's theory cannot make a firm prediction of the effective temperature of any cool star, including red clump giants.

In order to be compared with observations, the effective temperature of a stellar model is converted to a color, like  $(V - I)$ , which introduces next theoretical step: model atmosphere. While these are ever more sophisticated and presumably accurate, ultimately the accuracy of the  $T_{\text{eff}}$  *vs.* color transformation has to be empirically verified. The same is true for the bolometric corrections. Note that the bolometric luminosity provided by stellar models is not sensitive to the value of mixing length parameter. However, the bolometric correction rests on model atmospheres and their empirical calibration.

Stochastic mass loss from red giant stars is believed to be responsible for the morphology of the horizontal branch (Rood 1973, Chiosi, Bertelli, and Bressan 1992). In other words, the amount of matter lost affects stellar radius and effective temperature, affecting the size of a loop the star makes in the CMD. Red clump giants have identical interior structure as classical horizontal branch stars and therefore their loops are also affected by the amount of mass loss. As the reason for the stochastic nature of mass loss is not known, the size of those loops cannot be firmly predicted by the theory.

There is yet another major uncertainty of the models, which is not very well known, or not very well remembered. Several decades ago it was established that low mass stars develop large semiconvective zones just outside of their convective helium burning cores (Schwarzschild 1970, Iben 1974, and references therein). The question: "what is the proper criterion for a marginally stable gradient of chemical composition" was debated. There

has been no discussion of this subject lately, and there is no reference to the semiconvection in recent papers on models of horizontal branch or red clump stars. It is not clear whether the problem has been solved or forgotten.

Another very delicate issue is the extent to which chemical composition profile affects the size of the loops that stars make in the CMD while burning helium in their cores. Robertson (1971), and Lauterborn, Refsdal, and Weigert (1971) demonstrated that even very small changes in the stellar interior had a huge effect on the loop size. This is not important when the red clump models are very close to the red giant branch, *i.e.*, when the loop is very small, and the range of colors is very small. However, high metallicity clump models appear to have fairly extended loops (*cf.* Fig. 1 of Girardi *et al.* 1998), and the size of these may be very sensitive to many details of stellar structure.

The issue of the loop size can be most reliably resolved with the spectral observations, which may establish how tight (or not tight) is the correlation between the colors and metallicity of the red clump giants. The tighter the correlation, the smaller the loops have to be, and *vice versa*.

Considering the many difficulties with the stellar models it is not likely that they can provide quantities like  $M_I$  and  $(V - I)_0$  with a precision better than 0.1–0.2 mag, unless empirically calibrated. This is roughly the level at which the models and the observations appear to agree or disagree with each other.

### 6.3 Red Clump in the SMC

Although the Small Magellanic Cloud is not the topic of this paper, we present in Fig. 10 a color magnitude diagram for the red clump for a region near the south-west end of the SMC bar. We took the data from the SMC Photometric Maps published by the OGLE team (Udalski *et al.* 1998b), which have been accessible from the OGLE archive for over a year. The main reason for presenting Fig. 10 is to show how compact the red clump is when the reddening is not a problem, the range of distances is small, and the range of metallicities is low too. The data from the SMC maps may be useful to test and/or calibrate theoretical models. In particular, it is striking that the red clump in the SMC has no apparent structure, except for a cloud of stars above the main body of the clump; these are likely the younger and more massive stars as shown in Fig. 1 of Girardi *et al.* (1998).

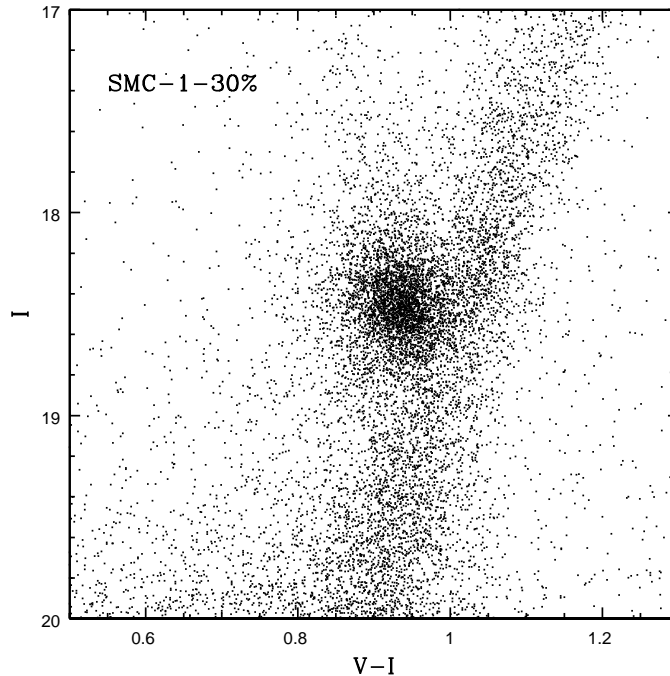


Fig. 10. Color-magnitude diagram for 30% of stars in the SMC field SMC\_SC1 (Udalski *et al.* 1998b). Note how narrow is the red giant branch and how compact is the red clump in this field with low and uniform reddening.

**Acknowledgments.** It is a great pleasure to acknowledge numerous discussions with Dr. K.Z. Stanek. We are very indebted to Dr. J.-C. Mermilliod for providing us with the *UBV* data for the Hipparcos stars in a computer readable form. We are very grateful to Dr. P. Popowski for pointing out some important omissions in the original version of this paper. We are also grateful to Dr. J. Cohen for pointing out mistakes in the original Table 3. This work was supported with the NSF grants AST-9530478 and AST-9820314 to B. Paczyński and the Polish KBN grant 2P03D00814 to A. Udalski.

## REFERENCES

- Alcock, C. *et al.* 1998, *Astrophys. J.*, **494**, 396.  
 Bertelli, G. *et al.* 1994, *Astron. Astrophys. Suppl. Ser.*, **106**, 275.  
 Caputo, F. *et al.* 1999, *Astron. J.*, **117**, 2199.  
 Chiosi, C., Bertelli, G., and Bressan, A. 1992, *Ann. Rev. Astron. Astrophys.*, **30**, 235.

- Girardi, L., Groenewegen, M.A.T, Weiss, A., and Salaris, M. 1998, *MNRAS*, **301**, 149.
- Girardi, L. 1999, astro-ph/9807086.
- Gould, A., Popowski, P., and Terndrup, D.M. 1998, *Astrophys. J.*, **492**, 778.
- Horner, D. *et al.* 1999, astro-ph/9907213.
- Iben, I.Jr. 1974, *Ann. Rev. Astron. Astrophys.*, **12**, 215.
- Jimenez, R., Flynn, C., and Kotoneva, E. 1998, *MNRAS*, **299**, 515.
- Kiraga, M., Paczyński, B., and Stanek, K.Z. 1997, *Astrophys. J.*, **485**, 611.
- Landolt, A.U. 1992, *Astron. J.*, **104**, 372.
- Lauterborn, D., Refsdal, S., and Weigert, A. 1971, *Astron. Astrophys.*, **10**, 97.
- Mermilliod, J.-C., and Mermilliod, M. 1994, "Catalogue of Mean *UBV* Data on Stars", Springer-Verlag.
- Paczyński, B. 1998, *Acta Astron.*, **48**, 405.
- Paczyński, B., and Stanek, K.Z. 1998, *Astrophys. J. Letters*, **494**, L219.
- Perryman, M.A.C. *et al.* 1997, *Astron. Astrophys.*, **323**, L49.
- Robertson, J.W. 1971, *Astrophys. J. Letters*, **164**, L105.
- Rood, R.T. 1973, *Astrophys. J.*, **184**, 815.
- Schwarzschild, M. 1970, *Quart. J. RAS*, **11**, 12.
- Sekiguchi, M., and Fukugita, M. 1999, astro-ph/9904299.
- Stanek, K.Z. 1996, *Astrophys. J.*, **460**, L37.
- Stanek, K.Z. and Garnavich, P. M. 1998, *Astrophys. J.*, **503**, 131.
- Stanek, K.Z., Zaritsky, D., and Harris, J. 1998, *Astrophys. J.*, **500**, 141.
- Stanek, K.Z., Kaluzny, J., Wysocka, A., and Thompson, I. 1999, astro-ph/9908041.
- Szymański, M., Udalski, A., Kubiak, M., Kaluzny, J., Mateo, M., and Krzemiński, W. 1996, *Acta Astron.*, **46**, 1.
- Udalski, A., Szymański, M., Kaluzny, J., Kubiak, M, and Mateo, M. 1993, *Acta Astron.*, **43**, 69.
- Udalski, A., Olech, A., Szymański, M., Kaluzny, J., Kubiak, M, Mateo, M. and Krzemiński, W. 1995, *Acta Astron.*, **45**, 433.
- Udalski, A., Kubiak, M., and Szymański, M. 1997, *Acta Astron.*, **47**, 319.
- Udalski, A. 1998a, *Acta Astron.*, **48**, 113.
- Udalski, A. 1998b, *Acta Astron.*, **48**, 383.
- Udalski, A., Szymański, M., Kubiak, M., Pietrzyński, G., Woźniak, P., and Żebruń, K. 1998a, *Acta Astron.*, **48**, 1.
- Udalski, A., Szymański, M., Kubiak, M., Pietrzyński, G., Woźniak, P., and Żebruń, K. 1998b, *Acta Astron.*, **48**, 147.